



MIT Open Access Articles

Relating transport modeling to nanofiltration membrane fabrication: Navigating the permeability-selectivity trade-off in desalination pretreatment

The MIT Faculty has made this article openly available. **Please share** how this access benefits you. Your story matters.

Citation	Labban, Omar et al. "Relating Transport Modeling to Nanofiltration Membrane Fabrication: Navigating the Permeability-Selectivity Trade-Off in Desalination Pretreatment." Journal of Membrane Science 554 (May 2018): 26–38 © 2018 Elsevier B.V.
As Published	http://dx.doi.org/10.1016/j.memsci.2018.02.053
Publisher	Elsevier
Version	Author's final manuscript
Accessed	Wed Apr 25 12:03:10 EDT 2018
Citable Link	http://hdl.handle.net/1721.1/114293
Terms of Use	Creative Commons Attribution-Noncommercial-Share Alike
Detailed Terms	http://creativecommons.org/licenses/by-nc-sa/4.0/

Relating Transport Modeling to Nanofiltration Membrane Fabrication: Navigating the Permeability-Selectivity Trade-off in Desalination Pretreatment

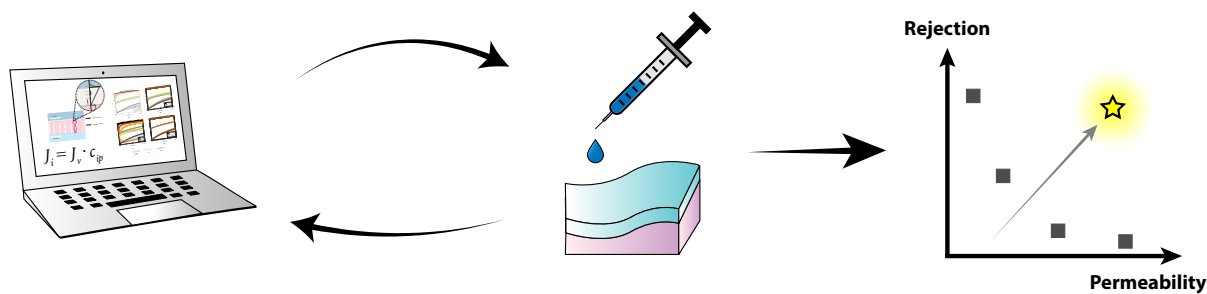
Omar Labban^a, Chang Liu^{b,c}, Tzyy Haur Chong^{b,c}, John H. Lienhard V^{a,*}

^aCenter for Clean Water and Clean Energy, Department of Mechanical Engineering, Massachusetts Institute of Technology, Cambridge MA 02139-4307, USA

^bSchool of Civil and Environmental Engineering, Nanyang Technological University, Singapore 639798, Singapore

^cSingapore Membrane Technology Centre, Nanyang Environment and Water Research Institute, Nanyang Technological University, Singapore 637141, Singapore

Abstract



Faced with a pressing need for membranes with a higher permeability and selectivity, the field of membrane technology can benefit from a systematic framework for designing membranes with the necessary physical characteristics. In this work, we present an approach through which transport modeling is employed in fabricating specialized nanofiltration membranes, that experimentally demonstrate enhanced selectivity. Specifically, the Donnan-Steric Pore Model with dielectric exclusion (DSPM-DE) is used to probe for membrane properties desirable in desalination pretreatment. Nanofiltration membranes are systematically fabricated in-house using layer-by-layer (LbL) deposition to validate model predictions and to develop a new specialized membrane for this application. The new membrane presents a 30% increase in permeability and a 50% reduction in permeate hardness relative to state-of-the-art NF membranes. Our results indicate that a ‘specialized’ tight membrane can outperform looser counterparts in both permeability and selectivity. Given the possibility of extending this framework to other applications, the work furthers our understanding of the relationships governing membrane form and function, while having broad potential implications for future nanofiltration membranes used in chemical separation and purification.

Keywords: permeability-selectivity trade-off, low-pressure nanofiltration, transport modeling, membrane fabrication, desalination pretreatment

*Corresponding author: lienhard@mit.edu

Nomenclature

Roman Symbols

A	Debye–Hückel constant, $\text{m}^{3/2}/\text{mol}^{1/2}$
A_m	Membrane permeability, $\text{L}/\text{m}^2 \cdot \text{h} \cdot \text{bar}$
A_k	Membrane porosity
c_i	Solute concentration of species i , mol/m^3
\tilde{c}_i	Solute concentration of species i , g/m^3
d_i	Fiber inside diameter, m
$D_{i,p}$	Diffusion coefficient of species i in the pore, m^2/s
$D_{i,\infty}$	Diffusion coefficient of species i in the bulk, m^2/s
e	Elementary charge, $1.60218 \times 10^{-19} \text{ C}$
F	Faraday constant, $96485.3 \text{ C}/\text{mol}$
I	Ionic strength, mol/m^3
J_i	Solute flux for species i , $\text{mol}/\text{m}^2 \cdot \text{s}$
J_v	Permeate flux, $\text{m}^3/\text{m}^2 \cdot \text{s}$
k	Boltzmann constant, $1.38065 \times 10^{-23} \text{ J}/\text{K}$
$k_{c,i}$	Solute mass transfer coefficient of species i , m/s
$K_{i,c}$	Convection hindrance factor of species i
$K_{i,d}$	Diffusion hindrance factor of species i
L	Module length, m
MW_i	Molecular weight for species i , mol/m^3
N	Identity of the N^{th} solute
N_A	Avogadro's number, $6.02214 \times 10^{23} \text{ mol}^{-1}$
Pe	Péclet number
r_i	Solute Stokes radius for species i , m
r_p	Effective pore radius, m
R	Universal gas constant, $8.31446 \text{ J}/\text{mol K}$
R_i	Rejection ratio of species i
R_h	Hardness removal
Re	Reynolds number
Sc	Schmidt number
Sh	Sherwood number
T	Temperature, K
V	Channel bulk velocity, m/s
x	Position across membrane active layer, m
X_d	Membrane charge density, mol/m^3

z_i Ion valency of species i

Greek Symbols

γ_i Activity coefficient of species i
 ΔP Applied pressure difference, Pa
 $\Delta \Pi$ Osmotic pressure difference, Pa
 ΔW_i Born solvation energy barrier, J
 Δx Thickness of membrane active layer, m
 ε_0 Permittivity of vacuum, 8.85419×10^{-12} F/m
 ε_b Relative permittivity/dielectric constant of the bulk
 ε_p Relative permittivity/dielectric constant of the pore
 ε_r Relative permittivity/dielectric constant
 λ_i Ratio of solute Stokes radius to effective pore radius of species i
 μ Solution viscosity, Pa · s
 ξ Electric potential gradient at the feed/membrane interface, V/m
 Ξ_i Mass transfer coefficient correction factor for species i
 ρ Solution density, kg/m³
 ϕ_i Ratio of permeate flux to the uncorrected mass transfer coefficient of species i
 Φ_i Steric partitioning coefficient of species i
 Φ_B Born solvation coefficient
 ψ Electric potential, V

Subscripts

b Bulk solution in the feed
 e Effective
 i Solute identity
 \lim Limiting rejection
 m Membrane
 p Membrane wall/permeate interface (just outside the membrane pores)
 p' Membrane wall/permeate interface (just inside the membrane pores)
 real Real rejection
 w Membrane wall/feed interface (just outside the membrane pores)
 w' Membrane wall/feed interface (just inside the membrane pores)

Superscripts

• Mass transfer correction for the suction effect

1. Introduction

Since the twentieth century, advances in membrane technology have been at the forefront of engineering innovations shaping humanity’s standard of living worldwide [1]. From medical applications such as drug delivery and tissue engineering [2] to industrial applications, ranging from gas separation [3] and water purification [4] to humidity harvesting and dehumidification [5], the importance of membranes to achieving chemical separation or moderated chemical transport cannot be overstated.

With great progress, however, came greater challenges to achieving high permeability without sacrificing selectivity as evident from the Robeson limit encountered in gas separation [6, 7] and the permeability-selectivity trade-off commonly reported in the desalination literature [8, 9, 10]. Ensuring optimal performance necessitates developing membranes that are tailored toward a given application. Systematic design of such membranes, however, requires a framework that relates the physical properties of membranes to their rejection characteristics.

The challenge is epitomized in desalination, where the drive for higher selectivity [9, 11, 12], as well as improved ion selectivity in pretreatment [13], is pivotal in tackling water scarcity, a global crisis among the most pressing of our time [14]. Standing as the most energy efficient desalination technology [15], reverse osmosis (RO) is plagued by inorganic fouling, for example, caused by hardness common to sea water and brackish waters [16].

Nanofiltration (NF) appears to offer a potential solution to hardness-related fouling, owing to its selective rejection of divalent ions relative to monovalent ions. In a work geared towards assessing the potential of NF in desalination pretreatment, Kaya et al. [17] experimentally evaluated the performance of different NF-RO configurations relative to single-stage RO, demonstrating improved permeate recovery as well as reduced RO scaling once NF was employed. Similarly, Macedonio et al. [18] quantitatively demonstrated, using energetic and exergetic arguments, that NF pretreatment can lower the energy consumption of desalination. These works, as well as others [19, 20, 21], underscore the potential of NF in desalination pretreatment. In the absence of commercial NF membranes specialized for this application, however, the benefits of NF pretreatment for RO feed water are expected to remain marginal.

In search of membranes better suited for the task, Fang et al. [22] pointed out that most commercial NF membranes are fabricated via the interfacial polymerization of piperazine (PIP) and trimesoyl chloride (TMC), leading to a negative surface charge that renders them ineffective at water softening. Setting the stage for a series of developments later in the field, Fang et al. [22] reported instead the fabrication of a novel low-pressure NF membrane by replacing PIP with branched polyethyleneimine (PEI), bringing about a more positive surface charge. The membrane demonstrated a unique softening capacity when operated at low pressure (2 bar), outperforming commercial competitors investigated at the time [22].

The study was followed by another by Liu et al. [23], who reported the fabrication of an alternative low-pressure NF membrane for water softening by semi-dynamic layer-by-layer (LbL) polyelectrolyte deposition. The membrane, fabricated by the deposition of poly(styrene sulfonate) or ‘PSS’ and poly(allylamine

hydrochloride) or ‘PAH’, consistently outperformed that of Fang et al. [22] from a hardness removal standpoint, although suffering in the presence of sulfate in the feed.

In response, Liu et al. [24] later introduced chemical crosslinking by glutaraldehyde (GA), producing a tighter membrane (LbL1.5C) that outperformed the preceding LbL membrane on both permeability and selectivity fronts, rejecting 80-100% of divalent ions with near-zero rejection of sodium ions in the feed. Such iterative efforts, among others [25], show the need for a systematic approach to guide membrane fabrication. The challenge is best summed in the words of a review on membrane fabrication by Laila et al. [26]: despite the existence of extensive knowledge on ‘tailoring’ membrane properties, a deeper understanding linking membrane properties to performance is crucial to the future progress of membrane technology in desalination — and arguably other fields.

With research on the solution-diffusion and pore-flow models dating back to the twentieth century [27, 28, 29], modeling chemical transport across membranes is as well established as the field of membrane technology. For decades, such efforts have primarily been channeled into understanding what mechanisms govern membrane transport [30, 31], predicting membrane performance [32], or designing large-scale membrane systems [33, 34, 35]. Less attention has been devoted to understanding how transport modeling can guide the fabrication of better membranes in light of two main limitations: (1) the lack of a ‘sufficiently detailed’ model relating membrane performance to its properties on the one hand; and (2) the need for an interdisciplinary effort spanning the distinct fields of membrane fabrication and transport modeling on the other hand. The need for a combined approach has become more evident as research heads in the direction of tailoring membranes for specific applications, as evident from other recent publications [10, 36, 37].

By coupling transport modeling to membrane fabrication, the present work takes an interdisciplinary approach toward a systematic framework, to our knowledge the first, that addresses this need. Desalination pretreatment by NF is chosen as the application of interest, with the objective of demonstrating the framework in the context of developing a specialized NF membrane for this application. Building on the preceding literature, the well-established Donnan-Steric Pore Model with dielectric exclusion (DSPM-DE), as presented by Geraldine and Alves [32], is adopted along with the LbL polyelectrolyte deposition [38] as our modeling and membrane modification tools of choice. With the LbL1.5C [24] serving as a benchmark, desirable membrane properties are probed by sensitivity analysis and experimentally validated by systematically fabricated membranes. Showing that a specialized membrane can enhance both permeability and ion selectivity, our work culminates in the development of a superior low-pressure membrane (LbL3), and demonstrates that transport modeling could systematically be employed to benefit membrane fabrication in the lab.

2. Theoretical Background

To relate modeling and fabrication, a ‘sufficiently detailed’ transport model should be adopted as a first step. The Donnan-Steric Pore Model with dielectric exclusion (DSPM-DE), used in nanofiltration and

adopted in this work, offers a more comprehensive treatment of membranes than other models (such as the Spiegler-Kedem model), characterizing them in terms of different properties, including the pore size, thickness, porosity, charge, and pore dielectric constant. Employing such a model is important as it offers a clearer understanding of the effect varying a fabrication procedure could have on membrane properties and performance later on.

This section begins with a brief overview of the DSPM-DE model and its governing equations. The limitations model calibration have traditionally imposed on modeling are then discussed, along with the exciting prospects that fitting parameters could offer when treated as design parameters to guide membrane fabrication. Thereafter, more formal definitions of ‘specialized performance’ and ‘low-pressure operation’ are laid out. With clear definitions, the section turns to assessing the merits and limits of different approaches to uncovering desirable membrane properties through modeling, and concludes by adopting sensitivity analysis as the approach of choice.

2.1. Governing equations of NF

Modeling transport across NF membranes is generally a three-step process that considers: solute transport within the active layer, concentration polarization, and solute partitioning at electrochemical equilibrium [13]. Figure 1 provides an illustration of a typical NF membrane in operation. Within the active layer, solute transport is governed by the extended Nerst-Planck equation, describing transport due to diffusion, convection, and electromigration [39]:

$$J_i = -D_{i,p} \frac{dc_i}{dx} + K_{i,c} c_i J_v - \frac{z_i c_i D_{i,p} F}{RT} \frac{d\psi}{dx} \quad (1)$$

$$D_{i,p} = K_{i,d} D_{i,\infty} \quad (2)$$

with J_i being the flux of the i^{th} solute, $D_{i,p}$ and $D_{i,\infty}$ its diffusion coefficient in the pore and the bulk solution, c_i its concentration, z_i its valency, J_v the permeate flux, and ψ the electric potential. F refers to the Faraday constant, R to the universal gas constant, and T to the temperature. Equation 1 indicates that transport occurs by virtue of the porosity of NF membranes, or down a gradient in concentration or electrical potential.

With length scales approaching those of atomic dimensions, solute mobility in the confining pores of NF membranes is restricted, the apparent rates of diffusion and convection are greatly reduced, and solute transport is said to be ‘hindered’ [40]. To account for hindered transport, the hindrance factors for diffusion $K_{i,d}$ and convection $K_{i,c}$ are introduced as shown in Eqs. 1-2. Details regarding the calculation of these factors can be found in Section S.1 of the Supporting Information. In addition to the extended Nerst-Planck equation, three electroneutrality conditions should also be satisfied within the active layer, at the feed/membrane interface, and in the permeate solution [32], and are provided in Section S.1.

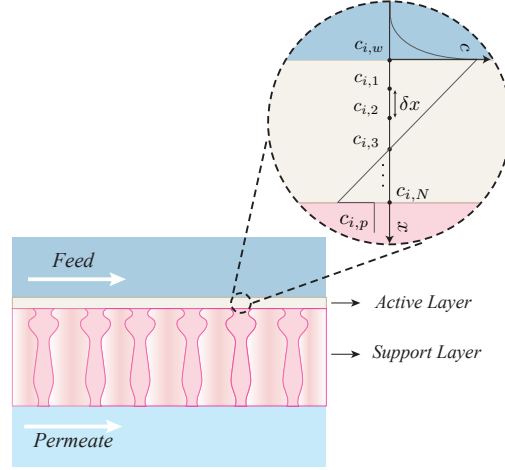


Figure 1: Modeling chemical transport through a NF membrane¹. The variables $c_{i,1}$ and $c_{i,N}$, appearing in the figure, match the variables $c_{i,w'}$ and $c_{i,p'}$ introduced in this work.

Apart from modeling transport within the active layer, concentration gradients tend to form across membrane interfaces as feed constituents permeate at differing rates (Fig. 1). This phenomenon, commonly referred to as concentration polarization (CP), impacts the permeate flux and quality, and should be considered. Following the model presented by Geraldes and Afonso, the solute flux across the CP layer at the feed/membrane interface can be expressed as the sum of fluxes due to back-diffusion, electromigration, and convection [41]:

$$J_i = -k_{c,i}^{\bullet}(c_{i,w} - c_{i,b}) + J_v c_{i,w} - z_i c_{i,w} D_{i,\infty} \frac{F}{RT} \xi \quad (3)$$

Here, the mass transfer coefficient is denoted as $k_{c,i}^{\bullet}$, $c_{i,b}$ and $c_{i,w}$ are the solute concentration in the bulk solution and at the membrane wall/feed interface (just outside the pores), and ξ refers to the gradient of electric potential at the interface. Details of the model and its assumptions are summarized in Section S.1. At steady state, the solute flux should also satisfy the conservation equation:

$$J_i = J_v c_{i,p} \quad (4)$$

The final step in modeling solute transport involves accounting for the solute partitioning that occurs at electrochemical equilibrium. Setting the electrochemical potential equal across both sides of a membrane interface yields two relationships, which act as boundary conditions at the feed/membrane and mem-

¹Reprinted from *Journal of Membrane Science*, 521, Labban et al., Fundamentals of low-pressure nanofiltration: Membrane characterization, modeling, and understanding the multi-ionic interactions in water softening, 18–32, Copyright (2017), with permission from Elsevier.

brane/permeate interfaces [32]:

$$\frac{\gamma_{i,w'}c_{i,w'}}{(\gamma_{i,w}c_{i,w})} = \Phi_i\Phi_B \exp\left(-\frac{z_iF}{RT}\Delta\psi_{D,w}\right) \quad (5)$$

$$\frac{\gamma_{i,p'}c_{i,p'}}{(\gamma_{i,p}c_{i,p})} = \Phi_i\Phi_B \exp\left(-\frac{z_iF}{RT}\Delta\psi_{D,p}\right) \quad (6)$$

These relationships describe solute partitioning as it occurs due to sieving (or size) effects, Donnan partitioning, and dielectric exclusion, all of which are important to membrane performance. In these equations, γ_i is the solute activity coefficient, Φ_i the steric partitioning coefficient, and Φ_B the Born solvation coefficient. Details on how these coefficients are calculated are addressed in Section S.1. The primed subscripts w' and p' here are used to denote the condition on the feed and permeate sides (just inside the membrane pores depicted in Fig. 1).

With these three steps accomplished, the membrane active layer is then discretized in the thickness direction as shown in Fig. 1, such that one extended Nerst-Planck equation is applied at every discretization point. The resulting system of equations is coupled to the boundary conditions (dictated by electrochemical equilibrium), electroneutrality conditions, and CP layer equations to numerically solve for the concentration profile. Our modeling approach is in tandem with that of Geraldles and Alves [32], and the reader is referred to another publication [13] for more details.

2.2. Fitting parameters: The limitation of traditional NF modeling

Developed over two decades, the DSPM-DE model adopted herein is well-established and has been extensively validated in the literature [32, 42, 43], and its applicability to the novel class of NF membranes developed by Liu et al. [24] has been demonstrated experimentally in a recent work [13]. Despite its great success, the need for calibration (or membrane characterization) has generally presented a limitation as evident from a study by Bowen and Mohammad [44], for example, solely dedicated to this purpose. Estimating a membrane's effective pore size, thickness, charge density, and dielectric constant through an expensive experimental protocol is always a requirement before any meaningful insights could be gleaned.

In this work, nonetheless, we pose the problem differently, looking at the model through the lens of a membrane designer. From a modeling standpoint, the performance of any membrane should be dictated by the four fitting parameters mentioned. Accordingly, the fitting parameter space can now be viewed as the membrane design space. Provided its assumptions are satisfied, the model can in principle be employed to probe which membrane properties are desirable for a specific application to achieve low-pressure operation. The path to implementing such an approach systematically remains ambiguous, however, without clear definitions for 'specialized' performance and 'low-pressure' operation.

2.3. Achieving low-pressure separation

In a critical study on modeling NF by the DSPM-DE model, Bowen and Welfoot [42] proved empirically that the permeate flux through the porous NF membranes is accurately predicted by the Hagen-Poiseuille

equation with a Staverman (reflection) coefficient of unity, and an effective driving pressure expressed as:

$$\Delta P_e = \Delta P - \Delta \Pi \quad (7)$$

where ΔP is the applied pressure and $\Delta \Pi$ the osmotic pressure difference. Rearranging their result to be expressed in terms of the applied pressure difference yields:

$$\Delta P = \frac{J_v}{A_m} + \Delta \Pi \quad (8)$$

$$A_m = \frac{r_p^2}{8\mu\Delta x_e} \quad (9)$$

with A_m being the membrane permeability as defined by Bowen and Welfoot [42]. In this derivation, μ refers to the solution viscosity, r_p to the effective pore radius, and Δx_e to the effective membrane thickness defined as the ratio of active layer thickness to porosity $\Delta x_e = \Delta x/A_k$. The osmotic pressure is calculated herein using van 't Hoff's equation.

Equation 8 has major implications on achieving low-pressure separation in practice. According to this result, two possibilities exist for membranes to operate under low-pressure (for a fixed flux J_v^*): increasing membrane permeability, A_m , or decreasing the osmotic pressure difference across the membrane, $\Delta \Pi$, by having improved ion selectivity that leaves a significant concentration of monovalent ions in both the feed and the permeate. In desalination pretreatment, where the focus is on hardness removal for example, improved selectivity implies 'selectively rejecting' the divalent ions Mg^{+2} and Ca^{+2} responsible for inorganic fouling, while passing low valence ions present in the feed, such as Na^+ and Cl^- . This unique ability of the LbL1.5C membrane, developed by Liu et al. [24], has already been shown to be responsible for its desirable low-pressure operation [13].

Permeability and rejection, however, are generally inversely related as evident from the permeability-selectivity trade-off encountered in practice [8, 9]. Figure 2 pictorially demonstrates the challenge encountered in membrane technology. 'Meaningful' low-pressure operation requires operation in the upper right-hand quadrant of the rejection-permeability plane. At the very least, either permeability or rejection should be increased while the other is held constant. Improving both permeability and rejection is a preferable alternative, albeit more challenging.

A membrane is said to be 'specialized' for a given application should its properties place it at a higher permeability-rejection frontier relative to alternatives, enabling 'low-pressure' operation. With this objective in mind, we next explore potential avenues by which transport modeling may guide membrane fabrication towards low-pressure operation.

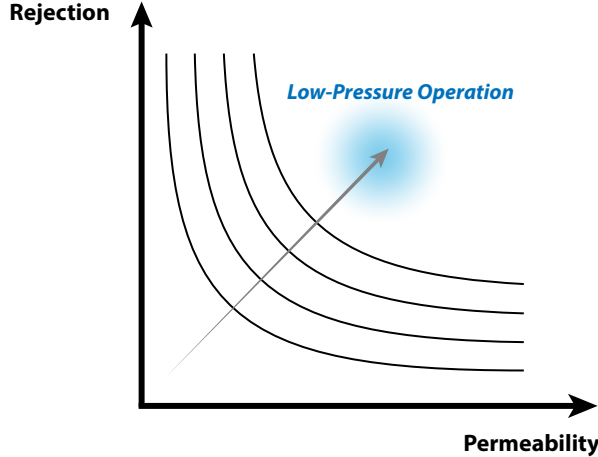


Figure 2: Permeability-selectivity trade-off encountered in practice.

2.4. Pathways to guiding membrane fabrication

Starting with a transport model, several pathways exist for uncovering the desirable characteristics a membrane should possess given an application. One option is numerical optimization [45], through which the membrane design space forms the parameter space for the optimization problem. The applied pressure difference is taken as the objective function to be minimized under the constraints that the permeate quality (or solute rejection) and flux fall within defined benchmarks. Based on an optimization algorithm, the solver starts from an initial guess for the desired membrane properties and solves the DSPM-DE model iteratively until convergence. While feasible, such an approach would be computationally expensive in light of the degrees of freedom existing and the variety of ions that may constitute the feed solution.

Parametric studies, on the other hand, offer the possibility of generating a master or surface plot on which optima can be located. With this approach, the applied pressure difference is plotted as a function of the different membrane characteristics for a fixed permeate flux and quality. Accordingly, the DSPM-DE model is then solved sequentially at all points of interest. Similar to numerical optimization, the procedure is likely to be computationally expensive. As an alternative, response surface methodology (RSM) could be used to generate a similar response plot based statistical methods using fewer test points [46]. The challenge of gleaning insightful conclusions from a five-dimensional array remains, however.

While all these techniques could in principle be employed to mathematically locate an optimum and predict desirable membrane properties, the greatest challenge will be ensuring that such an optimum is physically achievable: there is no guarantee that an actual membrane could embody the set of properties predicted, especially when those properties are coupled (e.g., tailoring thickness affects pore size).

To resolve these challenges, our study adopts sensitivity analysis to probe for desirable membrane characteristics given an application. Starting from a benchmark membrane, the method varies each property independently, probing the effect of different properties on membrane performance. Unlike other alternatives, sensitivity analysis is computationally cheap. Rather than search for an optimal set of characteristics,

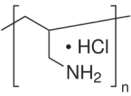
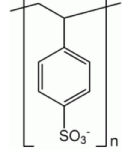
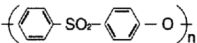
sensitivity analysis uncovers ‘trends’ that are easier to replicate in membrane fabrication. Given the focus of this work on improving membrane performance (as opposed to finding a mathematical optimum), these attributes make the method very attractive from an application standpoint. The method derives its validity from the model’s validity: under the condition that the model is valid and its assumptions are satisfied, the insights uncovered by this method should also be valid and satisfied.

3. Materials and methods

3.1. Materials and membranes

To prepare the polyelectrolyte solutions necessary for LbL deposition, poly(allylamine hydrochloride) (PAH, Sigma Aldrich, MW = 120-200 kDa), and poly(styrenesulfonic acid) sodium salt (PSS, Alfa Aesar, MW = 500 kDa) were used with sodium chloride (NaCl, Merck) as the supporting electrolyte (Table 1), and glutaraldehyde solution (GA, Sigma Aldrich, 50% in water) as the crosslinking agent. In preparing synthetic seawater, sodium chloride (NaCl), calcium chloride (CaCl_2), sodium sulfate (Na_2SO_4) and magnesium chloride (MgCl_2) were obtained from Merck.

Table 1: Chemical structure of polymers employed in LbL deposition.

Name	Acronym	Function	Chemical structure
Poly(allylamine hydrochloride)	(PAH)	Polyelectrolyte (poly-cation)	
Poly(styrene sulfonate)	(PSS)	Polyelectrolyte (poly-anion)	
Polyethersulfone	(PES)	Membrane substrate	

In addition, hydrochloric acid (HCl fuming 37%) and sodium hydroxide (NaOH) from Merck were employed in adjusting the pH of solutions. For uncharged solute rejection experiments, neutral organic solutes (ribose, glucose and sucrose) from Sigma Aldrich and Merck were also used. Deionized (DI) water was generated via a Milli-Q system (Millipore, USA).

The polyethersulfone (PES) ultrafiltration hollow fiber substrate and the polyelectrolyte-based selective layers with specific modifications were similar to the benchmark membrane LbL1.5C in our previous study [13]. The inner and outer diameters of the substrate are 1.0 and 1.4 mm, respectively, with the pure water permeability of around $350 \text{ L/m}^2 \cdot \text{h} \cdot \text{bar}$ and the molecular weight cut-off (MWCO) of 50 kDa.

3.2. LbL membrane preparation

While details of the layer-by-layer (LbL) deposition and the GA crosslinking are found in our previous studies [23, 24], a brief overview of the process is provided herein for completeness. First, the PES hollow

fiber substrates were fabricated in-house, and assembled into a coupon-sized module with an effective length of 24 cm. Polyelectrolyte layers, as well as GA crosslinking, were introduced with the help of a syringe into the fibers' interior. Alternating layers of PSS and PAH polyelectrolytes were applied for a predefined contact period (followed by a DI water rinse between the layers) until the desired number of layers was reached. Details regarding the specific concentration of polyelectrolytes and contact periods adopted for each of the membranes are provided in Section S.3 of the Supporting Information. The resulting membranes were then stored in DI water in preparation for filtration experiments.

Figure 3 schematically demonstrates the procedure and the different LbL membranes fabricated as part of this work. Guided by the modeling results, two types of LbL NF membranes, namely LbL1 and LbL2, were firstly fabricated to validate the effect of various properties on overall membrane performance. Inspired by both modeling and experimental validation results, LbL3 was further fine-tuned to be specialized for low-pressure seawater pretreatment with noticeable improvement in both water flux and hardness removal relative to the LbL1.5C benchmark as our work later demonstrates. Further details regarding the fabrication of these LbL membranes are provided in Section S.3, and briefly addressed later in Section 4.5 when analyzing the performance of the LbL3 relative to others. The NF270 membrane (DOW Filmtech) was adopted herein as a proxy for an unspecialized membrane.

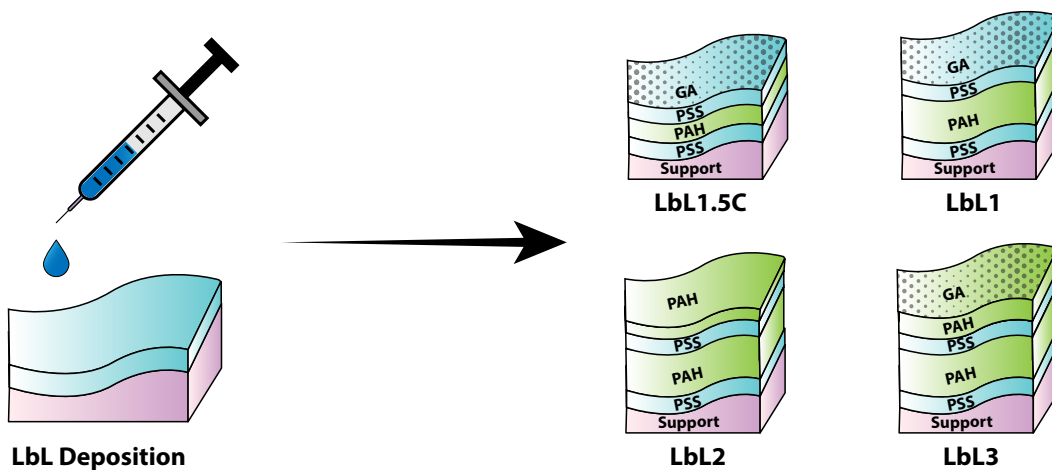


Figure 3: Schematic of the LbL deposition procedure and membranes fabricated (not to scale).

3.3. Nanofiltration experiments

Filtration experiments were conducted using a cross-flow filtration setup with applied pressures varying from 1 to 4 bar and a crossflow velocity maintained at 0.3 m/s to counteract the effects of concentration polarization. For uncharged solute rejection experiments, solutions of ribose, glucose, and sucrose with a concentration of 200 mg/kg were used. Single salt rejection experiments, required for membrane characterization as discussed in the next section, were performed with sodium chloride (NaCl) at a concentration of 1000 mg/kg and a pH varying from 5 to 10. Synthetic seawater was prepared following the concentrations

reported in Table 2.

Table 2: Synthetic seawater composition and charged solute properties (pH = 6.5).

	Na ⁺	Ca ⁺²	Mg ⁺²	SO ₄ ²⁻	Cl ⁻
r_i (nm)	0.184	0.309	0.347	0.230	0.121
D_∞ (m ² /s $\times 10^{-9}$)	1.33	0.792	0.706	1.06	2.03
Ion Concentration (mg/kg)	11122	382	1394	2136	20300

Total organic carbon measurements of the feed and permeate, conducted with a TOC analyzer (TOC-VCSH, Shimadzu, Japan), were used in determining uncharged solute rejection. Likewise, conductivity measurements of the feed and permeate with a conductivity meter (Ultrameter II, Myron L Company, Canada) were performed to determine single salt rejections. For synthetic seawater, inductively coupled plasma optical emission spectrometry (ICP-OES, Optima 8000, Perkin Elmer, USA) of the feed and permeate was employed in measuring ion rejections. Rejection tests were performed on two membrane modules, and average values were adopted.

3.4. Membrane Characterization

In this work, we adopt the membrane characterization method described in detail in our previous study [13]. The method requires four experiments for a given membrane to characterize the effective pore size, thickness, charge density, and pore dielectric constant. The procedure starts by fitting the effective pore size and thickness using pure water permeability and uncharged solute test results. The membrane charge density and dielectric constant are then determined based on single salt and synthetic seawater test results. The reader is referred to Section S.2 of the Supporting Information for more details on the membrane characterization procedure.

4. Results and discussion

With a transport model, a membrane modification procedure, and a framework based on sensitivity analysis in hand, this section analyzes the results of the experiments. Hardness removal is defined as the target metric and the LbL1.5C as the benchmark membrane. Modeling results investigating the effect of membrane properties on performance are presented and validated. Based on the insights uncovered, a new specialized membrane, the LbL3, is prepared and is shown to outperform the benchmark.

4.1. Target metric and benchmark definitions

The process of achieving a specialized membrane begins with the adoption of a target metric and a benchmark membrane, providing a basis for fair comparison. Considering applications to desalination pre-treatment and water softening, hardness removal, R_h , is selected herein as the target metric. As commonly

expressed in terms of the concentration of CaCO_3 , hardness offers a single value summing the concentrations of calcium and magnesium [47]. The result is a target metric, R_h , providing a measure of the total hardness removed from the system:

$$R_h = 1 - \frac{\left(\frac{\tilde{c}_{Ca} \times MW_{CaCO_3}}{MW_{Ca}} + \frac{\tilde{c}_{Mg} \times MW_{CaCO_3}}{MW_{Mg}} \right)_p}{\left(\frac{\tilde{c}_{Ca} \times MW_{CaCO_3}}{MW_{Ca}} + \frac{\tilde{c}_{Mg} \times MW_{CaCO_3}}{MW_{Mg}} \right)_f} \quad (10)$$

Here, \tilde{c}_i is the solute concentration in g/m^3 , MW the molecular weight in g/mol , and the subscripts p and f refer to the permeate and feed, respectively.

The LbL1.5C membrane, developed by Liu et al. [24] for water softening and desalination pretreatment, is adopted herein as the benchmark membrane given its superior performance. The LbL1.5C is a highly selective NF membrane fabricated in-house using layer-by-layer (LbL) polyelectrolyte deposition of a 1.5 bilayer (PSS/PAH/PSS) with glutaraldehyde (GA) crosslinking on top. Recently, the membrane was shown to achieve an 80 – 90% hardness rejection when treating synthetic seawater below 4 bar pressure [13]. By establishing the LbL1.5C as the benchmark, this work seeks to enhance its performance in light of insights uncovered by transport modeling, as we demonstrate next.

4.2. Modeling results

4.2.1. Effect of membrane thickness

To simplify the analysis, we initially adopt a pure water feed to investigate the effect of structural parameters on pure water permeability. Under the assumption of uniform cylindrical pores, the Hagen-Poiseuille equation may be used to relate the pure water flux to the membrane’s structural properties [44, 48, 49]:

$$J_v = \frac{r_p^2 \Delta P}{8\mu \Delta x_e} \quad (11)$$

where the symbols are defined identically to Eqs. 8-9. Recent experiments confirmed the applicability of this equation to the LbL1.5C membrane [13].

Following this definition, Fig. 4 depicts the change in pure water permeability, A_m , as a function of the effective pore size and thickness. As expected, the permeability increases with increasing pore size and decreasing thickness. A more subtle point, however, is the role played by thickness as an ‘attenuating’ or ‘amplifying’ factor for the flux. For a fixed change in pore size, the observed change in permeability is amplified with $\Delta x_e < 1 \mu\text{m}$ as captured by Fig. 4. While this result underscores the potential of ultra-thin membranes, it does not capture the effect of lower thickness on selectivity and rejection.

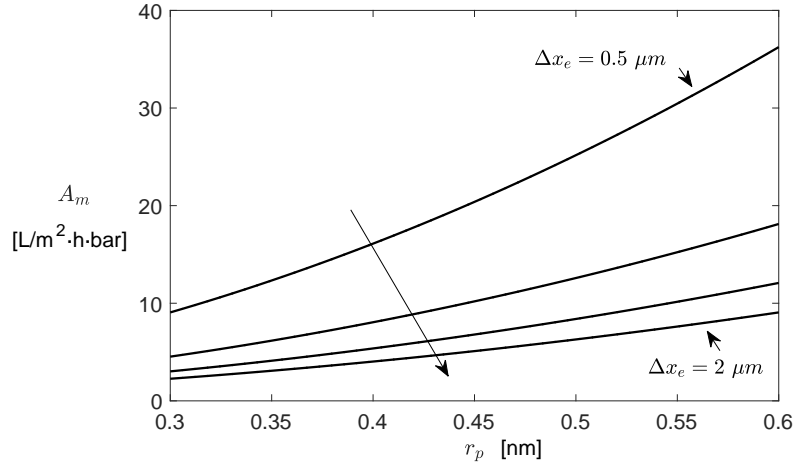


Figure 4: Membrane pure water permeability as a function of structural properties.

To examine the effect of membrane thickness on selectivity, hardness reduction, and applied pressure, a sensitivity analysis was applied to the benchmark membrane, holding all parameters constant, including seawater permeate flux at $J_v^* = 1 \times 10^{-6} \text{ m/s} = 3.6 \text{ L/m}^2\cdot\text{h}$, while varying thickness. This fixed flux is approximately the average achieved by the LbL1.5C under 3 bar pressure when treating synthetic seawater [13].

Figure 5 shows the predicted change in performance with effective thickness. From a fabrication standpoint, the effective thickness maybe increased by increasing the active layer's thickness or decreasing its porosity. Acting as a barrier to ion transport, increasing effective thickness improves rejection across all ions in the feed as demonstrated by Fig. 5a. Consequently, tuning this property appears less attractive as a means of tuning membrane selectivity among the feed constituent ions. The improvement is shown to be limited, diminishing with effective thickness.

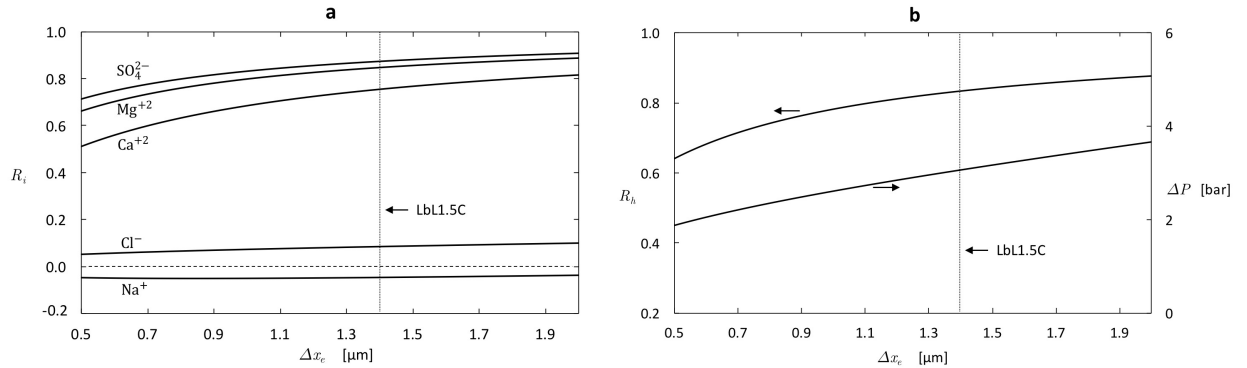


Figure 5: Predicted effect of thickness on membrane performance: (a) Ion rejection (b) Hardness removal and applied pressure required to maintain a constant permeate flux of $J_v^* = 1 \times 10^{-6} \text{ m/s} = 3.6 \text{ L/m}^2\cdot\text{h}$.

Figure 5b depicts the predicted hardness removal for a given effective thickness. The trend reported follows that of the underlying multivalent ions, increasing with effective thickness and underscoring the diminishing returns likely to be encountered. According to Fig. 5b, the applied pressure necessary to provide the target flux J_v^* grows almost linearly with effective thickness. Since permeability is linear in effective thickness, Eq. 8 indicates the effect of diminishing permeability dominates that of increasing osmotic pressure, suggesting the effective thickness at higher values primarily acts as an impediment to flux. To summarize, reducing effective thickness offers the opportunity of improved permeability without dramatically sacrificing membrane rejection of the LbL1.5C.

Another observation to note from Fig. 5a is the occurrence of negative rejection. This phenomenon, which has been well-documented in the literature [50, 51, 52], will also be encountered in the upcoming simulation and experimental results. In an earlier work [13], we successfully modeled the performance of the LbL1.5C in an attempt to provide a detailed account of its unique performance, including the negative rejection of certain ions. A brief explanation addressing this phenomenon will be provided in this section for completeness, and the reader is referred to existing literature for more details.

Negative rejection occurs when the permeate concentration exceeds that of the feed for any given solute in the system. The phenomenon, resulting from the interactions between the ions and the membrane, does not violate mass conservation. Instead, the different ions are allocated among the feed and the smaller permeate volume, such that mass conservation is always satisfied.

The negative rejection of Na^+ observed in Fig. 5a may be explained by assuming the membrane is impermeable to divalent ions. As Cl^- (whose concentration is the largest in the system) faces little retention by the membrane, it travels down its gradient in electrochemical potential with Na^+ as the only counter-ion available to neutralize the feed and permeate solutions. Accordingly, Na^+ is ‘effectively pulled’ by the Cl^- to satisfy charge electroneutrality constraints. This effect results in a greater permeate concentration of Na^+ than would otherwise occur, bringing about the occurrence of negative rejection.

4.2.2. *Effect of membrane charge*

Figure 6 demonstrates the predicted change in membrane performance for the LbL1.5C in response to changing membrane charge. In practice, charge may be manipulated per application requirements through a membrane modification process, such as polyelectrolyte deposition, coating, or grafting [53]. As shown in Fig. 6a, the response experienced makes it evident that charge, unlike effective thickness, may be tailored to enhance membrane selectivity among the different ions. While divalent cation rejection improved with positively increasing charge in response to electrostatic interactions and enhanced Donnan exclusion, divalent anion rejection decreased. Given the focus of the current study on hardness removal and desalination pretreatment, the change appears favorable as indicated by Fig. 6b and in agreement with earlier reports by Liu et al. [24, 23] and Fang et al. [22].

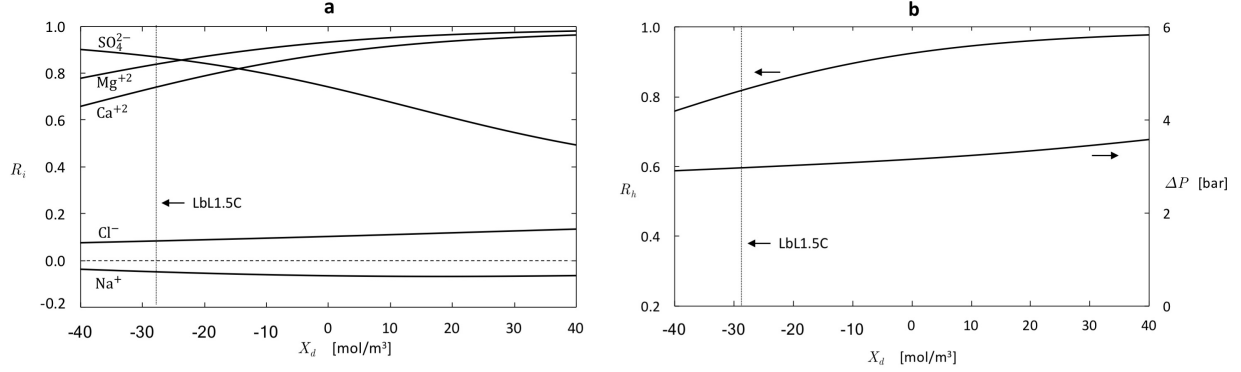


Figure 6: Predicted effect of charge density on membrane performance: (a) Ion rejection (b) Hardness removal and applied pressure required to maintain a constant permeate flux of $J_v^* = 1 \times 10^{-6}$ m/s = 3.6 L/m²·h.

Despite the observed improvement in hardness removal, the expected change in applied pressure is relatively insignificant as Fig. 6b demonstrates. This finding is corroborated by the trade-off taking place between divalent cation and anion retentions as membrane selectivity is modified. Although membrane charge spanned a huge range in the simulations, hardness removal was not as sensitive to charge variation (relative to pore size variation as we demonstrate later). At the upper extreme in Fig. 6b, membrane charge actually became notably less effective at improving hardness rejection. The diminishing returns observed are reflective of the exponentially decaying Donnan partitioning term in Eq. 5. As membrane charge becomes more positive, the Donnan potential at the feed/membrane interface, $\Delta\psi_{D,w}$, increases monotonically such that any further increase in the Donnan partitioning effect becomes exponentially less noticeable.

The observation that hardness removal is not a strong function of membrane charge makes it evident that, in this case, membrane charge might not be the preferred property to modify in search of improved performance. As such, a membrane designer, targeting the LbL1.5C membrane for enhanced desalination pretreatment, is better served by a moderately positive charge ($X_d \sim 10 - 20$ mol/m³) at which point charge becomes less effective, while instead manipulating the effective pore size, as we discuss next.

4.2.3. Effect of membrane pore size

Holding thickness and charge constant, Fig. 7 shows the change in membrane performance with varying pore size. A membrane may be made tighter and more selective through a membrane modification process, such as chemical cross-linking [24, 54]. As different ions are influenced to varying degrees, Fig. 7a indicates that pore size may also be used to tune a membrane's ion selectivity.

In contrast to monovalent ions, all divalent ion rejections increased as the membrane became tighter. The observed improvement in divalent ion rejection, however, ceased once the pore size dropped below $r_p^* \sim 0.4$ nm. Another interesting insight comes from the order of ions affected by the pore size change. Since the LbL1.5C membrane appeared negatively charged at the feed conditions considered [13], sulfate rejection was impacted the least and always exceeded that of other divalent ions. On the other hand, due to its higher

diffusivity and lower Stokes radius relative to magnesium, calcium rejection dropped the most with pore size.

More importantly, hardness removal, as apparent from Fig. 7b, was highly sensitive to changes in pore size. In fact, a small pore size change entails a sizable hardness removal boost without a significant loss of permeability, a result that we will leverage to improve both permeability and selectivity. As the pore size continues dropping, nonetheless, a critical pore size is encountered, beyond which changes in monovalent ion rejections start playing a prominent role. As shown in Fig. 7b, the applied pressure necessary to provide the benchmark flux rises in conjunction with the higher rejections for monovalent ions. Since these ions constitute the majority of the feed solution, the chemical separation process is heavily penalized by the rising osmotic pressure and falling permeability, such that the applied pressure starts approaching values typical of reverse osmosis [55].

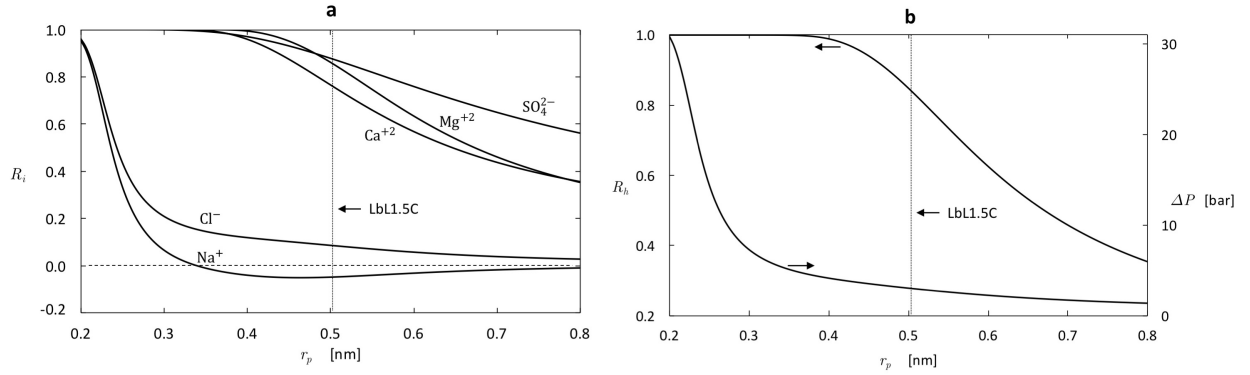


Figure 7: Predicted effect of pore size on membrane performance: (a) Ion rejection (b) Hardness removal and applied pressure required to maintain a constant permeate flux of $J_v^* = 1 \times 10^{-6}$ m/s = 3.6 L/m²·h.

To summarize this section, our modeling results indicated that lowering the effective thickness improves permeability without drastically reducing rejection. Furthermore, a positive membrane charge was found to be beneficial to hardness removal, albeit with diminishing returns at higher values. Additionally, hardness removal was found to be highly sensitive to the pore size. Decreasing the pore size improved the rejection of divalent ions until a critical pore size was reached, beyond which a greater energy penalty was incurred with increasing monovalent ion rejection. In light of these takeaways, Table 3 summarizes the desired range for each of the parameters considered based on modeling results to achieve enhanced selectivity in desalination pretreatment.

Table 3: Summary of model recommendations, taking the LbL1.5C as a benchmark and synthetic seawater (Table 2) as feed water, for enhanced selectivity.

Parameter	Recommended Range
Δx_e (μm)	$< 1 \mu\text{m}$
X_d (mol/m^3)	$\sim 20 \text{ mol}/\text{m}^3$
r_p (nm)	$\sim 0.4 \text{ nm}$

4.2.4. Effect of membrane pore dielectric constant

Our study, thus far, has analyzed the effect of the effective thickness, charge, and pore size on membrane performance in desalination pretreatment. Before transitioning to the validation of the recommendations presented, we offer here a brief overview of the predicted effect of the pore dielectric constant, the last membrane parameter in our model.

As shown in Fig. 8a, rejection across all ions drops with increasing pore dielectric constant. With an increase in the pore dielectric constant, ions experience a lower barrier to solvation as predicted by Born model, bringing about lower rejections. Given the dependency of the Born solvation energy barrier on ion valency (Section S.1 - Supporting Information), divalent ion rejection is seen to be more sensitive to a change in the pore dielectric constant relative to monovalent ion rejection. Below a threshold value ($\epsilon_p \sim 35$), however, monovalent ion rejection becomes significant. Notably, the effect of the constant on membrane performance can be considerable, and comparable to that of pore size.

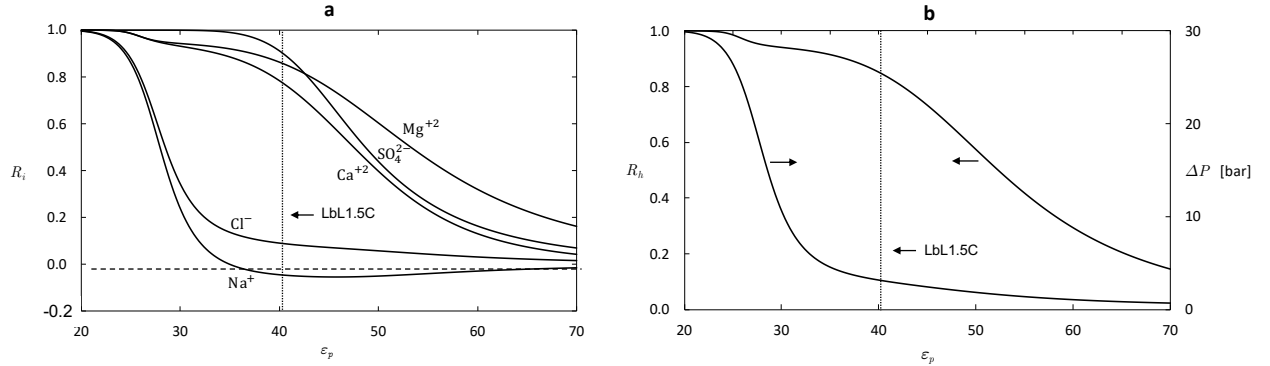


Figure 8: Predicted effect of the pore dielectric constant on membrane performance: (a) Ion rejection (b) Hardness removal and applied pressure required to maintain a constant permeate flux of $J_v^* = 1 \times 10^{-6} \text{ m/s} = 3.6 \text{ L}/\text{m}^2 \cdot \text{h}$.

Figure 8b depicts the effect of the pore dielectric constant on hardness removal and applied pressure. As the pore dielectric constant is varied from its benchmark value, hardness removal is seen to be highly sensitive to the pore dielectric constant, a trend matched by the underlying ions. Similar to the effect of pore size, applied pressure increases monotonically as the constant decreases, approaching values common to RO when monovalent ion rejection becomes considerable.

While this work has controlled membrane thickness, charge, and pore size (in light of existing literature) to fabricate a specialized membrane, we could not control the pore dielectric constant. In the next section, experimental results are employed in validating the predicted effects of thickness, charge, and pore size on membrane performance in desalination pretreatment. A discussion of any potential effect the pore dielectric constant might have had on our recommendations and results is discussed in Section 4.5.3.

4.3. Experiments and validation

4.3.1. Membrane selection

To validate the results of Section 4.2, two membranes, the LbL1 and LbL2, were purposely fabricated with differing properties using layer-by-layer deposition as discussed in Section 3.2. These membranes, whose properties are summarized in Table 4, were characterized following the method we outlined earlier in Section 3.4.

Table 4: Membrane characterization parameters.

Membrane	r_p (nm)	Δx_e (μm)	ε_p	X_d (mol/m^3)
LbL1.5C	0.51	1.33	41	-27
LbL1	0.48	0.72	44	-39
LbL2	0.60	1.25	47.5	20
LbL3	0.46	0.78	45	23
NF270	0.49	0.79	44	-56

As shown in Table 4, the membranes were chosen to differ considerably from the LbL1.5C to allow for a meaningful comparison. This objective is easily achieved by altering one or more of the deposition conditions in light of the high flexibility of the LbL modification process. Relative to the LbL1.5C, the LbL1, for example, featured a high PAH polymer concentration to form more fixed-polymer pairs on the membrane surface (instead of unpaired curved fragments) [56, 57]. Consequently, the LbL1 had a lower effective thickness (almost 50% lower) while the pore size remained relatively constant, albeit a bit smaller. In sharp contrast, the LbL2 had a larger pore size (notably looser) and the reverse charge (strongly positive) compared to the LbL1.5C, while possessing a relatively similar effective thickness. In this case, a positively charged PAH layer was adopted as the capping layer without GA crosslinking, such that the resultant membrane was positively charged with a looser pore structure. (The design of the LbL3 membrane will be discussed in Section 4.5).

The properties of the LbL1 make it ideal for evaluating the effect of thickness on membrane performance. As a looser and positively charged membrane, the LbL2, on the other hand, is uniquely positioned to evaluate whether a tighter membrane would be desired in desalination pretreatment as predicted earlier. Our fabrication work shows the difficulty associated with controlling membrane properties. Unlike modeling,

whereby only one property is allowed to vary, variation in one property during fabrication should be expected to cause a slight variation in other properties given practical limitations on membrane fabrication and the coupling that exists between the membrane properties.

4.3.2. Performance evaluation

Once the LbL1 and LbL2 membranes were selected, experiments were run on all membranes following the protocol laid out in Section 3.3. Pure water permeability, uncharged solute rejection, single salt rejection, and synthetic seawater rejection tests were all performed. Given the focus of this work on desalination pretreatment, however, we limit our discussion to pure water permeability and seawater rejection results.

Figure 9 depicts the experimental results obtained for pure water permeability. As shown, both membranes (LbL1 and LbL2) yielded a higher flux compared to the LbL1.5C. For the LbL1, permeability increased from 10 L/m²·h·bar to approximately 16 L/m²·h·bar (60% increase). The observation is inline with modeling predictions as the membrane’s effective thickness was about half that of the LbL1.5C. Similarly, the LbL2, whose pore size exceeded that of the LbL1.5C, demonstrated a 50% increase in permeability reaching 15 L/m²·h·bar.

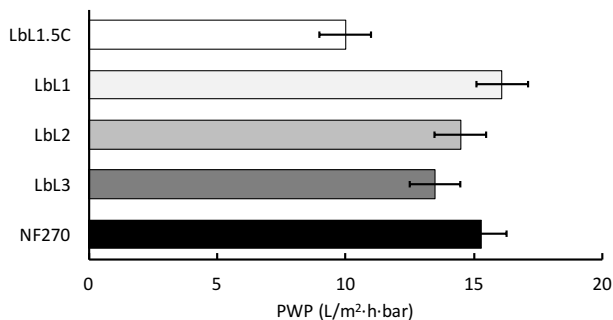


Figure 9: Performance test results: Pure water permeability (PWP).

More importantly, Fig. 10 reports the results obtained for hardness removal from synthetic seawater experiments at an applied pressure of 4 bar. As shown for the LbL1, permeate flux almost doubled relative to the LbL1.5C (increasing from 6 L/m²·h to 13 L/m²·h) as effective thickness was halved. Unlike permeate flux, hardness removal, nevertheless, remained relatively constant. The observation is important as it provides evidence that selectivity among the ions is not a strong function of effective thickness as suggested by the transport model. By leveraging the high sensitivity of permeability to thickness (with $\Delta x_e < 1 \mu\text{m}$) coupled with a relatively stable hardness removal predicted by the model, the LbL1 not only outperforms the benchmark LbL1.5C, but actually stands out already as a considerable improvement over it.

For the LbL2, the permeate flux similarly increased relative to the LbL1.5C as the pore sized was increased. In spite of its positive charge, hardness removal surprisingly deteriorated. The fact that a loose membrane was outperformed by a tighter less positive membrane, the LbL1, is significant as it indicates

that permeability increased at the expense of ion selectivity and validates experimentally our prediction that hardness removal is highly sensitive to pore size.

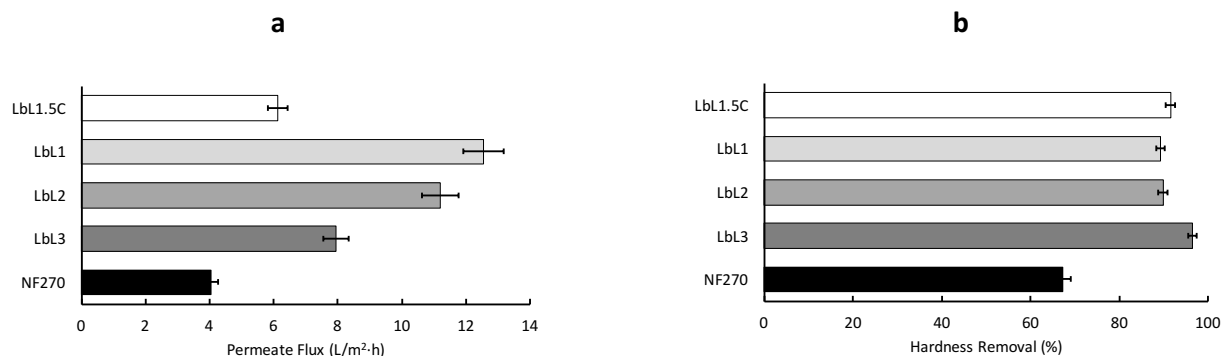


Figure 10: Synthetic seawater test results at 4 bar: (a) Permeate flux (b) Hardness removal.

To offer a more detailed perspective, Fig. 11 compares the rejections for all multivalent ions composing the feed solution at 4 bar applied pressure. Compared to the LbL1.5C, the LbL1 had a very similar rejection profile. Calcium rejection decreased more notably than magnesium's given the membrane's higher negative charge and the ion's smaller Stokes radius and larger diffusivity. In contrast, the LbL2 retention for sulfate decreased most notably as the membrane became positively charged. As the pore size was increased, magnesium and more noticeably calcium rejections also decreased, rendering the membrane less effective overall at hardness removal and desalination pretreatment.

In short, the results reported in this section validate the trends predicted earlier by the transport model. Together, the modeling and experimental results highlight what membrane properties are desirable for desalination pretreatment. In the next section, we revisit the main takeaways of our analysis before we discuss the preparation of the LbL3.

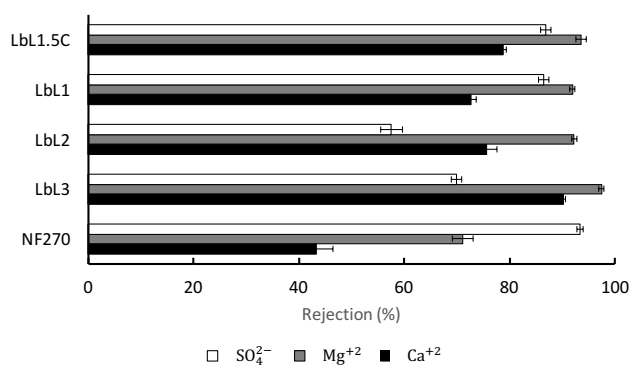


Figure 11: Synthetic seawater test results at 4 bar: Individual divalent ion rejections.

4.4. Takeaways from modeling and experimental results

With modeling results analyzed and validated experimentally, we may summarize the main takeaways from our analysis, and how it could be employed to offer a pathway to specialized membrane performance in desalination pretreatment. First, our results have demonstrated that membrane effective thickness strongly influences permeability without significantly impacting hardness removal or ion selectivity.

Moreover, a high membrane charge density ‘in isolation’ was shown to be less effective at boosting performance and improving selectivity in light of the diminishing returns predicted with increasing charge. A moderately positive charge ($X_d \sim 10 - 20 \text{ mol/m}^3$), however, was still found to be beneficial in this case as it improved hardness removal. Most importantly, pore size was shown to play a dominant role in dictating a membrane’s selectivity for divalent ions.

Together, these insights suggest that an ideal membrane for desalination pretreatment should combine: (1) a low barrier to permeate flux through a lower effective thickness; (2) a higher ion selectivity through a moderately positive charge; and (3) a ‘sufficiently tight’ pore structure to effectively block divalent cations. In the next section, we present our approach to preparing such a membrane, and discuss how its performance fares relative competitors investigated in our study.

4.5. Pathway to a specialized membrane

4.5.1. LbL3 membrane preparation

Successfully fabricating a membrane, which possesses the specifications outlined, requires understanding what effect the different deposition conditions have had on membrane characteristics. In fabricating the different membranes, the LbL composition and PAH concentration were the only two factors allowed to vary in this work. Accordingly, Fig. 3 and Table 5 summarize the LbL composition and PAH concentration for each membrane, along with the observed membrane properties. The acronyms “PSS” and “PAH” refer to the polyelectrolytes “poly(styrene sulfonate)” and “poly(allylamine hydrochloride)” used in the LbL deposition process, while “GA” refers to “glutaraldehyde” crosslinking.

Table 5: Summary of LbL fabricated membranes: Composition and properties (relative to the benchmark membrane).

Membrane	LbL composition	PAH concentration	Observed properties
LbL1.5C	(PSS/PAH/PSS) + GA	0.02 M	Benchmark membrane
LbL1	(PSS/PAH/PSS) + GA	0.1 M	Thinner
LbL2	PSS/PAH/PSS/PAH	0.1 M	Looser and more positive
LbL3	(PSS/PAH/PSS/PAH) + GA	0.1 M	Thinner, tighter and more positive

As reported by Liu et al. [24] and summarized in Table 5, the benchmark LbL1.5C was fabricated by the deposition of a 1.5 bilayer (PSS/PAH/PSS) with glutaraldehyde crosslinking. Increasing the concentration of PAH led to a decrease in effective thickness demonstrated by the LbL1 by forming more fixed-polymer

pairs on the surface, an effect discussed in Section 4.3.1. Since a lower thickness was found to be desirable in our application, a similar concentration of PAH was adopted for all subsequent membranes. Capping the membrane with an additional layer of PAH led to a more positive charge density for the LbL2 in the presence of more amine groups, albeit the pore structure was looser given the absence of glutaraldehyde crosslinking.

To prepare a membrane with the desired specifications relative to the LbL1.5C (thinner, more positive, and tighter), a higher concentration of PAH was adopted in conjunction with an additional capping layer of PAH with glutaraldehyde crosslinking as shown in Table 5. Depositing an additional PAH layer relative to LbL1.5C (prior to glutaraldehyde crosslinking) provided additional reaction sites (NH_2 groups from PAH), leading to an even tighter pore structure. Membrane characterization results reported in Table 4 confirm that the LbL3 successfully possesses all three specifications required, suggesting that the membrane should outperform the benchmark LbL1.5C.

4.5.2. *LbL3 membrane testing*

We next look at the experimental performance of the new membrane relative to the benchmark LbL1.5C and NF270, taken as a proxy for an unspecialized off-the-shelf membrane. Detailed experimental results for the LbL3 covering uncharged solutes, single salts, and synthetic seawater as part of the study are all provided in Section S.4 of the Supporting Information. These results may be compared to a similar set reported for the LbL1.5C in an earlier work [13] to offer a more holistic picture. Given the scope of this work, however, we limit the discussion in this section to desalination pretreatment.

Starting with Fig. 9, experimental results demonstrate the LbL3 achieved around 30% higher pure water permeability (PWP) relative to the LbL1.5C in spite of its tighter pore structure. The observation is significant as it demonstrates how thickness may be leveraged to improve permeability while still achieving a tighter pore structure and higher selectivity, a result predicted earlier in Section 4.2. Interestingly, NF270 fared well relative to most membranes on the PWP front. As an unspecialized membrane, nonetheless, NF270 was at a significant disadvantage when handling synthetic seawater as our results demonstrate.

Figure 10 depicts the experimental results obtained for the treatment of synthetic seawater. First, the LbL3 achieved the highest hardness removal among all membranes considered in the study, while still delivering a comparable flux ($\sim 8 \text{ L/m}^2\cdot\text{h}$) at 4 bar. Achieving a 30% higher permeability and a 50% reduction in permeate hardness, the performance of the LbL3 indicates an improvement on both permeability and ion selectivity fronts relative to the benchmark, proving ultimately the feasibility of employing transport modeling to further membrane fabrication. In contrast, the notably poor performance of NF270 serves as a reminder of the disadvantages that unspecialized membranes can bring to a given application.

A more detailed understanding may be gleaned from Fig. 11. Among all membranes investigated, the LbL3 attained the highest retention of calcium and magnesium. Overall, the LbL3 retained less sulfate, compared to the benchmark, by virtue of its charge. Finally, we note that the highly negative charge of NF270 led to its drastically poor performance, coming full circle to the observation first made by Fang et al. [22].

4.5.3. *Effect of the variation in the pore dielectric constant*

As the pore dielectric constant was not controlled, we end this study by showing that the variation in the pore dielectric constant, while observed experimentally, does not undercut our recommendations for the LbL3. Starting with the benchmark LbL1.5C in Table 4, the LbL1 featured a relative increase in the pore dielectric constant. Since hardness removal remained relatively stable, the relative increase in the dielectric constant could only have subverted our first recommendation to lower thickness had it been associated with improved performance. In contrast, an increase in pore dielectric constant is expected to decrease performance, so our finding that hardness removal is less sensitive to effective thickness is not challenged by this variation in the dielectric constant between LbL1.5C and LbL1.

Moving on to our second recommendation on charge, both the LbL1 and NF270 exhibited similar pore sizes and thicknesses, and more importantly, had the same dielectric constant. The only major difference among the two membranes lies in charge. The fact that the LbL1, which featured a more positive charge, outperformed NF270 suggests that the preference towards a more positive charge in desalination pretreatment holds as well.

On our third recommendation to decrease pore size, comparing the LbL2 and LbL3 shows that both of them possessed a similar charge. Featuring a smaller pore size, dielectric constant, and thickness, the LbL3 demonstrated a considerably higher hardness removal relative to the LbL2. As hardness removal deteriorates with decreasing thickness, the significant boost in performance is attributed either to the smaller pore size or smaller dielectric constant. Since the pore size varied more significantly among the two membranes, we conclude its effect in this case is likely to have been dominant, consistent with our third recommendation.

Accordingly, our comparison of the different membranes reveals that, in spite of the experimentally observed variation in the pore dielectric constant, our fabrication recommendations for the LbL3 still hold. In light of the high sensitivity of the membrane hardness removal to the pore dielectric constant as revealed in Section 4.2.4, however, future work should explore potential avenues of controlling this parameter, or modifying it with fabrication techniques as a means of tailoring membrane performance.

5. Conclusions

A framework relating transport modeling to membrane fabrication was presented, taking the Donnan-Steric Pore Model with dielectric exclusion (DSPM-DE) and the semi-dynamic layer-by-layer (LbL) polyelectrolyte deposition as the transport model and the membrane modification tools of choice. Focusing on desalination pretreatment, analytical variations of membrane physical properties were used to define fabrication parameters that achieve high ion selectivity during low pressure operation. The work culminated in the development of a new specialized membrane, the LbL3, offering a 30% increase in permeability and a 50% reduction in permeate hardness relative to our benchmark membrane when treating synthetic seawater.

The key results of this study are:

1. Transport modeling can be employed in guiding membrane fabrication to develop better membranes, demonstrating higher permeability and ion selectivity.
2. A ‘specialized’ tight membrane could outperform looser versions in both permeability and selectivity.
3. Our model is highly consistent with expected trends, such as the effect of thickness on performance, but allows for rational design of membranes to better tune those trends.
4. Unlike thickness, membrane charge can be employed in tuning ion selectivity. Hardness removal improves with increasingly positive charge, albeit with diminishing returns reflective of the exponentially decaying nature of the Donnan partitioning effect.
5. Pore size dictates a membrane’s rejection and selectivity more than thickness or charge.
6. The extremely high sensitivity of rejection to pore size may be leveraged in carefully boosting rejection without considerably sacrificing flux, especially when combined with a reduced thickness.
7. For desalination pretreatment, a membrane should ideally combine: (i) a lower effective thickness, (ii) a moderately positive charge density, and (iii) a sufficiently tight pore structure. Possessing all three attributes, the LbL3 outperformed the benchmark membrane and achieved the highest hardness removal among all membranes considered.

Acknowledgements

This research is supported by the National Research Foundation (NRF) Singapore under its Campus for Research Excellence and Technological Enterprise (CREATE) programme. The Center for Environmental Sensing and Modeling (CENSAM) is an interdisciplinary research group (IRG) of the Singapore MIT Alliance for Research and Technology (SMART) centre. The Singapore Membrane Technology Centre (SMTC) is supported by the Economic Development Board (EDB) of Singapore. The authors acknowledge Professor Wang Rong of SMTC and Yagnaseni Roy for their input and support of this work.

References

- [1] R. W. Baker, Membrane Technology and Applications, John Wiley & Sons, Ltd, 2004. doi:10.1002/0470020393.
URL <http://dx.doi.org/10.1002/0470020393>
- [2] D. F. Stamatialis, B. J. Papenburg, M. Gironés, S. Saiful, S. N. Bettahalli, S. Schmitmeier, M. Wessling, Medical applications of membranes: Drug delivery, artificial organs and tissue engineering, Journal of Membrane Science 308 (1–2) (2008) 1 – 34. doi:<https://doi.org/10.1016/j.memsci.2007.09.059>.
URL <http://www.sciencedirect.com/science/article/pii/S0376738807007090>
- [3] P. Bernardo, E. Drioli, G. Golemme, Membrane gas separation: A review/state of the art, Industrial & Engineering Chemistry Research 48 (10) (2009) 4638–4663. arXiv:<http://dx.doi.org/10.1021/ie8019032>, doi:10.1021/ie8019032.
URL <http://dx.doi.org/10.1021/ie8019032>
- [4] A. G. Fane, R. Wang, M. X. Hu, Synthetic membranes for water purification: Status and future, Angewandte Chemie International Edition 54 (11) (2015) 3368–3386. doi:10.1002/anie.201409783.
URL <http://dx.doi.org/10.1002/anie.201409783>
- [5] O. Labban, T. Chen, A. F. Ghoniem, J. H. Lienhard V, L. K. Norford, Next-generation HVAC: Prospects for and limitations of desiccant and membrane-based dehumidification and cooling, Applied Energy 200 (2017) 330 – 346. doi:10.1016/j.apenergy.2017.05.051.
URL <http://www.sciencedirect.com/science/article/pii/S0306261917305160>
- [6] L. M. Robeson, Correlation of separation factor versus permeability for polymeric membranes, Journal of Membrane Science 62 (2) (1991) 165 – 185. doi:10.1016/0376-7388(91)80060-J.
URL <http://www.sciencedirect.com/science/article/pii/037673889180060J>
- [7] L. M. Robeson, The upper bound revisited, Journal of Membrane Science 320 (1–2) (2008) 390 – 400. doi:10.1016/j.memsci.2008.04.030.
URL <http://www.sciencedirect.com/science/article/pii/S0376738808003347>
- [8] G. M. Geise, H. B. Park, A. C. Sagle, B. D. Freeman, J. E. McGrath, Water permeability and water/salt selectivity tradeoff in polymers for desalination, Journal of Membrane Science 369 (1–2) (2011) 130 – 138. doi:10.1016/j.memsci.2010.11.054.
URL <http://www.sciencedirect.com/science/article/pii/S0376738810009233>
- [9] J. R. Werber, A. Deshmukh, M. Elimelech, The critical need for increased selectivity, not increased water permeability, for desalination membranes, Environmental Science & Technology Letters 3 (4) (2016) 112–120. arXiv:<http://dx.doi.org/10.1021/acs.estlett.6b00050>, doi:10.1021/acs.estlett.

6b00050.

URL <http://dx.doi.org/10.1021/acs.estlett.6b00050>

- [10] H. B. Park, J. Kamcev, L. M. Robeson, M. Elimelech, B. D. Freeman, Maximizing the right stuff: The trade-off between membrane permeability and selectivity, *Science* 356 (6343). [arXiv:http://science.sciencemag.org/content/356/6343/eaab0530.full.pdf](https://arxiv.org/abs/http://science.sciencemag.org/content/356/6343/eaab0530.full.pdf), doi:10.1126/science.aab0530.
URL <http://science.sciencemag.org/content/356/6343/eaab0530>
- [11] D. Cohen-Tanugi, R. K. McGovern, S. H. Dave, J. H. Lienhard V, J. C. Grossman, Quantifying the potential of ultra-permeable membranes for water desalination, *Energy Environ. Sci.* 7 (2014) 1134–1141. doi:10.1039/C3EE43221A.
- [12] R. K. McGovern, J. H. Lienhard V, On the asymptotic flux of ultrapermeable seawater reverse osmosis membranes due to concentration polarisation, *Journal of Membrane Science* 520 (2016) 560 – 565. doi:10.1016/j.memsci.2016.07.028.
URL <http://www.sciencedirect.com/science/article/pii/S0376738816309656>
- [13] O. Labban, C. Liu, T. H. Chong, J. H. Lienhard V, Fundamentals of low-pressure nanofiltration: Membrane characterization, modeling, and understanding the multi-ionic interactions in water softening, *Journal of Membrane Science* 521 (2017) 18 – 32. doi:http://dx.doi.org/10.1016/j.memsci.2016.08.062.
URL <http://www.sciencedirect.com/science/article/pii/S0376738816307050>
- [14] M. M. Mekonnen, A. Y. Hoekstra, Four billion people facing severe water scarcity, *Science Advances* 2 (2). doi:10.1126/sciadv.1500323.
URL <http://advances.sciencemag.org/content/2/2/e1500323>
- [15] K. H. Mistry, R. K. McGovern, G. P. Thiel, E. K. Summers, S. M. Zubair, J. H. Lienhard, Entropy generation analysis of desalination technologies, *Entropy* 13 (10) (2011) 1829–1864.
- [16] S. Shirazi, C.-J. Lin, D. Chen, Inorganic fouling of pressure-driven membrane processes — a critical review, *Desalination* 250 (1) (2010) 236 – 248. doi:10.1016/j.desal.2009.02.056.
URL <http://www.sciencedirect.com/science/article/pii/S0011916409007541>
- [17] C. Kaya, G. Sert, N. Kabay, M. Arda, M. Yüksel, Özdemir Egemen, Pre-treatment with nanofiltration (NF) in seawater desalination—Preliminary integrated membrane tests in Urla, Turkey, *Desalination* 369 (2015) 10 – 17. doi:10.1016/j.desal.2015.04.029.
URL <http://www.sciencedirect.com/science/article/pii/S0011916415002829>
- [18] F. Macedonio, E. Curcio, E. Drioli, Integrated membrane systems for seawater desalination: Energetic and exergetic analysis, economic evaluation, experimental study, *Desalination* 203 (1) (2007) 260 – 276.

doi:10.1016/j.desal.2006.02.021.

URL <http://www.sciencedirect.com/science/article/pii/S0011916406012756>

- [19] Y. Song, X. Gao, T. Li, C. Gao, J. Zhou, Improvement of overall water recovery by increasing R_{NF} with recirculation in a NF–RO integrated membrane process for seawater desalination, *Desalination* 361 (2015) 95 – 104. doi:10.1016/j.desal.2015.01.023.
URL <http://www.sciencedirect.com/science/article/pii/S0011916415000429>
- [20] W. L. Ang, A. W. Mohammad, N. Hilal, C. P. Leo, A review on the applicability of integrated/hybrid membrane processes in water treatment and desalination plants, *Desalination* 363 (2015) 2 – 18, Hybrid Systems for Desalination. doi:10.1016/j.desal.2014.03.008.
URL <http://www.sciencedirect.com/science/article/pii/S0011916414001337>
- [21] L. Llenas, X. Martínez-Lladó, A. Yaroshchuk, M. Rovira, J. de Pablo, Nanofiltration as pretreatment for scale prevention in seawater reverse osmosis desalination, *Desalination and Water Treatment* 36 (1-3) (2011) 310–318.
- [22] W. Fang, L. Shi, R. Wang, Interfacially polymerized composite nanofiltration hollow fiber membranes for low-pressure water softening, *Journal of Membrane Science* 430 (2013) 129 – 139. doi:10.1016/j.memsci.2012.12.011.
URL <http://www.sciencedirect.com/science/article/pii/S0376738812009210>
- [23] C. Liu, L. Shi, R. Wang, Enhanced hollow fiber membrane performance via semi-dynamic layer-by-layer polyelectrolyte inner surface deposition for nanofiltration and forward osmosis applications, *Reactive and Functional Polymers* 86 (2015) 154 – 160. doi:10.1016/j.reactfunctpolym.2014.07.018.
URL <http://www.sciencedirect.com/science/article/pii/S138151481400145X>
- [24] C. Liu, L. Shi, R. Wang, Crosslinked layer-by-layer polyelectrolyte nanofiltration hollow fiber membrane for low-pressure water softening with the presence of SO_4^{2-} in feed water, *Journal of Membrane Science* 486 (2015) 169 – 176. doi:10.1016/j.memsci.2015.03.050.
URL <http://www.sciencedirect.com/science/article/pii/S0376738815002380>
- [25] L. Setiawan, L. Shi, R. Wang, Dual layer composite nanofiltration hollow fiber membranes for low-pressure water softening, *Polymer* 55 (6) (2014) 1367 – 1374. doi:10.1016/j.polymer.2013.12.032.
URL <http://www.sciencedirect.com/science/article/pii/S0032386113011324>
- [26] B. S. Lalia, V. Kochkodan, R. Hashaikeh, N. Hilal, A review on membrane fabrication: Structure, properties and performance relationship, *Desalination* 326 (2013) 77 – 95. doi:10.1016/j.desal.2013.06.016.
URL <http://www.sciencedirect.com/science/article/pii/S0011916413003093>

- [27] P. Meares, On the mechanism of desalination by reversed osmotic flow through cellulose acetate membranes, *European Polymer Journal* 2 (3) (1966) 241 – 254. doi:10.1016/0014-3057(66)90045-0.
URL <http://www.sciencedirect.com/science/article/pii/0014305766900450>
- [28] G. Thau, R. Bloch, O. Kedem, Water transport in porous and non-porous membranes, *Desalination* 1 (2) (1966) 129 – 138. doi:10.1016/S0011-9164(00)84012-6.
URL <http://www.sciencedirect.com/science/article/pii/S0011916400840126>
- [29] A. S. Michaels, H. J. Bixler, R. M. Hodges, Kinetics of water and salt transport in cellulose acetate reverse osmosis desalination membranes, *Journal of Colloid Science* 20 (9) (1965) 1034 – 1056. doi:
[http://dx.doi.org/10.1016/0095-8522\(65\)90072-3](http://dx.doi.org/10.1016/0095-8522(65)90072-3).
URL <http://www.sciencedirect.com/science/article/pii/0095852265900723>
- [30] A. E. Yaroshchuk, Dielectric exclusion of ions from membranes, *Advances in Colloid and Interface Science* 85 (2–3) (2000) 193 – 230. doi:10.1016/S0001-8686(99)00021-4.
URL <http://www.sciencedirect.com/science/article/pii/S0001868699000214>
- [31] Y. Roy, D. M. Warsinger, J. H. Lienhard V, Effect of temperature on ion transport in nanofiltration membranes: Diffusion, convection and electromigration, *Desalination* 420 (2017) 241 – 257. doi:<https://doi.org/10.1016/j.desal.2017.07.020>.
URL <http://www.sciencedirect.com/science/article/pii/S0011916417304745>
- [32] V. Geraldes, A. M. B. Alves, Computer program for simulation of mass transport in nanofiltration membranes, *Journal of Membrane Science* 321 (2) (2008) 172 – 182. doi:10.1016/j.memsci.2008.04.054.
URL <http://www.sciencedirect.com/science/article/pii/S037673880800392X>
- [33] W. N. Gill, B. Bansal, Hollow fiber reverse osmosis systems analysis and design, *AIChE Journal* 19 (4) (1973) 823–831. doi:10.1002/aic.690190422.
URL <http://dx.doi.org/10.1002/aic.690190422>
- [34] Y. Roy, M. H. Sharqawy, J. H. Lienhard V, Modeling of flat-sheet and spiral-wound nanofiltration configurations and its application in seawater nanofiltration, *Journal of Membrane Science* 493 (2015) 360 – 372. doi:10.1016/j.memsci.2015.06.030.
URL <http://www.sciencedirect.com/science/article/pii/S0376738815300028>
- [35] O. Labban, T. H. Chong, J. H. Lienhard V, Design and modeling of novel low-pressure nanofiltration hollow fiber modules for water softening and desalination pretreatment, Under Review.
- [36] M. A. Alaei Shahmirzadi, S. S. Hosseini, G. Ruan, N. R. Tan, Tailoring PES nanofiltration membranes through systematic investigations of prominent design, fabrication and operational parameters, *RSC*

Adv. 5 (2015) 49080–49097. doi:10.1039/C5RA05985B.

URL <http://dx.doi.org/10.1039/C5RA05985B>

- [37] X. Q. Cheng, C. Zhang, Z. X. Wang, L. Shao, Tailoring nanofiltration membrane performance for highly-efficient antibiotics removal by mussel-inspired modification, *Journal of Membrane Science* 499 (2016) 326 – 334. doi:10.1016/j.memsci.2015.10.060.
URL <http://www.sciencedirect.com/science/article/pii/S037673881530288X>
- [38] Y. Lvov, G. Decher, H. Moehwald, Assembly, structural characterization, and thermal behavior of layer-by-layer deposited ultrathin films of poly(vinyl sulfate) and poly(allylamine), *Langmuir* 9 (2) (1993) 481–486. doi:10.1021/la00026a020.
- [39] W. R. Bowen, J. S. Welfoot, P. M. Williams, Linearized transport model for nanofiltration: Development and assessment, *AIChE Journal* 48 (4) (2002) 760–773. doi:10.1002/aic.690480411.
URL <http://dx.doi.org/10.1002/aic.690480411>
- [40] W. M. Deen, Hindered transport of large molecules in liquid-filled pores, *AIChE Journal* 33 (9) (1987) 1409–1425. doi:10.1002/aic.690330902.
URL <http://dx.doi.org/10.1002/aic.690330902>
- [41] V. Geraldes, M. D. Afonso, Prediction of the concentration polarization in the nanofiltration/reverse osmosis of dilute multi-ionic solutions, *Journal of Membrane Science* 300 (1–2) (2007) 20 – 27. doi:10.1016/j.memsci.2007.04.025.
URL <http://www.sciencedirect.com/science/article/pii/S0376738807002815>
- [42] W. Bowen, J. S. Welfoot, Modelling the performance of membrane nanofiltration—critical assessment and model development, *Chemical Engineering Science* 57 (7) (2002) 1121 – 1137. doi:10.1016/S0009-2509(01)00413-4.
URL <http://www.sciencedirect.com/science/article/pii/S0009250901004134>
- [43] T. Tsuru, S. Nakao, S. Kimura, Calculation of ion rejection by extended Nernst–Planck equation with charged reverse osmosis membranes for single and mixed electrolyte solutions, *Journal of Chemical Engineering of Japan* 24 (4) (1991) 511–517. doi:10.1252/jcej.24.511.
- [44] W. Bowen, A. Mohammad, Characterization and prediction of nanofiltration membrane performance—a general assessment, *Chemical Engineering Research and Design* 76 (8) (1998) 885 – 893, Separation Processes. doi:10.1205/026387698525685.
URL <http://www.sciencedirect.com/science/article/pii/S0263876298717253>
- [45] U. Diwekar, Introduction to applied optimization, Vol. 22, Springer Science & Business Media, 2008.

- [46] A. I. Khuri, S. Mukhopadhyay, Response surface methodology, Wiley Interdisciplinary Reviews: Computational Statistics 2 (2) (2010) 128–149. doi:10.1002/wics.73.
URL <http://dx.doi.org/10.1002/wics.73>
- [47] P. Brezonik, W. Arnold, Water chemistry: An introduction to the chemistry of natural and engineered aquatic systems, Oxford University Press, New York, 2011.
- [48] W. Bowen, A. Mohammad, N. Hilal, Characterisation of nanofiltration membranes for predictive purposes — use of salts, uncharged solutes and atomic force microscopy, Journal of Membrane Science 126 (1) (1997) 91 – 105. doi:10.1016/S0376-7388(96)00276-1.
URL <http://www.sciencedirect.com/science/article/pii/S0376738896002761>
- [49] W. Bowen, A. Wahab Mohammad, Diafiltration by nanofiltration: Prediction and optimization, AIChE Journal 44 (8) (1998) 1799–1812. doi:10.1002/aic.690440811.
URL <http://dx.doi.org/10.1002/aic.690440811>
- [50] W. Bowen, H. Mukhtar, Characterisation and prediction of separation performance of nanofiltration membranes, Journal of Membrane Science 112 (2) (1996) 263 – 274. doi:10.1016/0376-7388(95)00302-9.
URL <http://www.sciencedirect.com/science/article/pii/0376738895003029>
- [51] T. Tsuru, M. Urairi, S.-I. Nakao, S. Kimura, Negative rejection of anions in the loose reverse osmosis separation of mono-and divalent ion mixtures, Desalination 81 (1-3) (1991) 219–227.
- [52] A. E. Yaroshchuk, Negative rejection of ions in pressure-driven membrane processes, Advances in Colloid and Interface Science 139 (1–2) (2008) 150 – 173, membrane Electrochemistry: Selected papers from the 33rd Conference on Membrane Electrochemistry, Russia, May 2007. doi:10.1016/j.cis.2008.01.004.
URL <http://www.sciencedirect.com/science/article/pii/S0001868608000328>
- [53] N. Hilal, A. F. Ismail, C. Wright, Membrane Fabrication, CRC Press, 2015.
- [54] J. L. Stair, J. J. Harris, M. L. Bruening, Enhancement of the ion-transport selectivity of layered polyelectrolyte membranes through cross-linking and hybridization, Chemistry of Materials 13 (8) (2001) 2641–2648. doi:10.1021/cm010166e.
- [55] L. D. Banchik, M. H. Sharqawy, J. H. Lienhard V, Effectiveness-mass transfer units (ε -*MTU*) model of a reverse osmosis membrane mass exchanger, Journal of Membrane Science 458 (2014) 189 – 198. doi:10.1016/j.memsci.2014.01.039.
URL <http://www.sciencedirect.com/science/article/pii/S0376738814000520>
- [56] S. T. Dubas, J. B. Schlenoff, Factors controlling the growth of polyelectrolyte multilayers, Macromolecules 32 (24) (1999) 8153–8160. doi:10.1021/ma981927a.

- [57] M. Michel, V. Toniazzo, D. Ruch, V. Ball, Deposition mechanisms in layer-by-layer or step-by-step deposition methods: From elastic and impermeable films to soft membranes with ion exchange properties, ISRN Materials Science 2012 (2012) doi:10.5402/2012/701695.